ARL-TN-0784 ● SEP 2016

US Army Research Laboratory

Molecular Simulations of Shear-Induced Dynamics in Nitromethane

by Brad A Steele and James P Larentzos

Approved for public release; distribution is unlimited.

NOTICES

Disclaimers

The findings in this report are not to be construed as an official Department of the Army position unless so designated by other authorized documents.

Citation of manufacturer's or trade names does not constitute an official endorsement or approval of the use thereof.

Destroy this report when it is no longer needed. Do not return it to the originator.

ARL-TN-0784 ● SEP 2016

US Army Research Laboratory

Molecular Simulations of Shear-Induced Dynamics in Nitromethane

by Brad A Steele
University of South Florida, Department of Physics, Tampa, Florida

James P Larentzos
Weapons and Materials Research Directorate, ARL

Approved for public release; distribution is unlimited.

REPORT DOCUMENTATION PAGE

Form Approved
OMB No. 0704-0188

Public reporting burden for this collection of information is estimated to average 1 hour per response, including the time for reviewing instructions, searching existing data sources, gathering and maintaining the data needed, and completing and reviewing the collection information. Send comments regarding this burden estimate or any other aspect of this collection of information, including suggestions for reducing the burden, to Department of Defense, Washington Headquarters Services, Directorate for Information Operations and Reports (0704-0188), 1215 Jefferson Davis Highway, Suite 1204, Arlington, VA 22202-4302. Respondents should be aware that notwithstanding any other provision of law, no person shall be subject to any penalty for failing to comply with a collection of information if it does not display a currently valid OMB control number.
PLEASE DO NOT RETURN YOUR FORM TO THE ABOVE ADDRESS.

1. REPORT DATE *(DD-MM-YYYY)*	2. REPORT TYPE	3. DATES COVERED (From - To)
September 2016	Technical Note	1 May–31 August 2016

4. TITLE AND SUBTITLE
Molecular Simulations of Shear-Induced Dynamics in Nitromethane

5a. CONTRACT NUMBER

5b. GRANT NUMBER

5c. PROGRAM ELEMENT NUMBER

6. AUTHOR(S)
Brad A Steele and James P Larentzos

5d. PROJECT NUMBER
HIP-FY16-018

5e. TASK NUMBER

5f. WORK UNIT NUMBER

7. PERFORMING ORGANIZATION NAME(S) AND ADDRESS(ES)
US Army Research Laboratory
ATTN: RDRL-WML-B
Aberdeen Proving Ground, MD 21005-5069

8. PERFORMING ORGANIZATION REPORT NUMBER
ARL-TN-0784

9. SPONSORING/MONITORING AGENCY NAME(S) AND ADDRESS(ES)

10. SPONSOR/MONITOR'S ACRONYM(S)

11. SPONSOR/MONITOR'S REPORT NUMBER(S)

12. DISTRIBUTION/AVAILABILITY STATEMENT
Approved for public release; distribution is unlimited.

13. SUPPLEMENTARY NOTES

14. ABSTRACT
The atomistic dynamics of the shear response of single-crystal and bicrystal nitromethane (NM) are simulated using molecular dynamics simulations. The atomic interactions are described using a recently optimized ReaxFF-lg potential trained specifically for NM. We found that NM transforms to a disordered state upon shear at a pressure of 20 GPa and 298 K. Shear simulations of several different orientations show that the maximum shear stress and shear angle where the transformation to the disordered state occurs are highly dependent on the crystallographic orientation of NM. The dynamics that occur during shear in several different single-crystal orientations are elucidated. Shear simulations in bicrystal NM show more complex behavior, and the disordered state typically originates at the grain boundary and then grows. The shear response is simulated at pressures and temperatures where NM has been experimentally observed to undergo chemical decomposition when shear stress is applied. Although no reactions occur in these simulations, these results shed light on the short time scale reaction pathways that NM can take during shear-induced initiation.

15. SUBJECT TERMS
nitromethane, shear, molecular dynamics, LAMMPS, grain boundary

16. SECURITY CLASSIFICATION OF:			17. LIMITATION OF ABSTRACT	18. NUMBER OF PAGES	19a. NAME OF RESPONSIBLE PERSON
a. REPORT	b. ABSTRACT	c. THIS PAGE			James P Larentzos
Unclassified	Unclassified	Unclassified	UU	24	19b. TELEPHONE NUMBER (Include area code) 410-306-0809

Standard Form 298 (Rev. 8/98)
Prescribed by ANSI Std. Z39.18

Contents

Approved for public release; distribution is unlimited.

List of Figures

List of Tables

Approved for public release; distribution is unlimited.

Acknowledgments

This work is supported by the DOD High Performance Computing Modernization Program under grant number HIP-FY16-018. We would like to thank Shawn Coleman for providing his grain boundary builder code, which made most of these simulations possible. We also thank Betsy Rice, Tim Jenkins, and William Matson for their insightful discussions.

Approved for public release; distribution is unlimited.

INTENTIONALLY LEFT BLANK.

Approved for public release; distribution is unlimited.

1. Introduction

Nitromethane (NM) is one of the most widely studied insensitive energetic molecules.[1–8] The main reason for its popularity is that it is one of the simplest nitro-organic molecules containing only one nitro group (NO_2) bonded to one methyl group (CH_3) through a C-N bond. This makes it an ideal candidate to study chemical reaction mechanisms associated with conventional explosive initiation and subsequent detonation.[3,6,7] However, understanding the ultra-fast reaction mechanisms for initiation is challenging.

The study of initiation and chemical reaction mechanisms of mechanically stressed materials such as shock compression, hydrostatic compression, uniaxial compression, or shear is called mechanochemistry. The broad field of mechanochemistry applied to energetics covers a large range of conditions and interactions that can be potentially exploited for advanced energy release applications. In addition, mechanochemistry is also relevant for nonenergetics for phase transitions and chemical reactions that occur when mechanically stressed.

NM is a liquid at ambient pressure, but when compressed to about 0.3 GPa, it crystallizes in the $P2_12_12_1$ space group.[1] When hydrostatically compressed to 28 GPa, NM slowly decomposes to what is reported to be a 3-D disordered polymer.[2] In contrast, when NM is compressed to 28 GPa and then sheared, Raman studies show that the decomposition is sudden and explosive.[5] In addition, structural modifications are found to occur at a lower hydrostatic pressure when sheared in comparison to hydrostatic pressure alone.[5] One model that has been proposed to explain the explosive decomposition of NM under shear stress examines the orientation-dependent steric hindrance to shear flow at the molecular level.[4] It was found that certain orientations of NM are highly sterically hindered and are therefore more sensitive to chemical reactions and initiation than others. However, this is a static model that does not capture the dynamics that occur in the crystal during shear.[4]

In this work we examine the dynamics that occur during shear of NM by performing classical molecular dynamics simulations. The crystallographic orientation dependence on the shear response of NM is calculated. In addition, since there is a strong correlation between grain boundaries (GBs) and chemical initiation in energetic materials, bicrystalline NM with a GB is also simulated.

Approved for public release; distribution is unlimited.

2. Computational Details

Molecular dynamics simulations are performed using the LAMMPS (Large-scale Atomic/Molecular Massively Parallel Simulator) simulation package.[9] The interatomic interactions are described by the ReaxFF-lg potential recently created using the MOES (Multiple Objective Evolutionary Strategies) algorithm[10,11] and refitted to NM.[10–13] This potential shows good agreement to the experimental equation of state and melting lines for NM. Fully 3-D periodic crystals of NM in various orientations are generated using the GB builder code developed by Shawn Coleman (US Army Research Laboratory, Weapons and Materials Research Directorate) and initially relaxed in the NPT (constant number of atoms, pressure, and temperature) ensemble at 20 GPa and 298 K. Special care is taken to ensure the crystal structure generated by the code is equivalent to the original crystal structure. The crystals are then sheared in the microcanonical ensemble with a constant strain rate equal to 0.0008 ps^{-1} over a 100-ps time period. The strain rate is defined as offset divided by the length, where the length is the initial box length in the direction perpendicular to shear (e.g., the y box length for xy deformation), and the offset is the change in the direction in the shear direction (e.g., the change in the x box length for xy deformation). Each crystal is sheared along all 3 angles in the simulation box (xy, xz, and yz). The effect the strain rate has on the results is analyzed by performing simulations with a strain rate an order of magnitude higher and lower than 0.0008, and no significant deviations are found. Each orientation has a different number of atoms in the unit cell to ensure 3-D periodicity; however, all simulations use at least 20,000 atoms in a simulation box bigger than 35 × 35 × 35 $Å^3$. The number of atoms in the cell is also varied to ensure no significant size dependence on the results. Several hundred bicrystalline structures of NM are constructed using similar orientations used in the single crystal simulations and are initially relaxed at 20 GPa and 298 K. The bicrystalline structures are 2-D periodic in the xz plane while the size of the grain along the y axis is 100 Å (both grains are 100 Å). Simulations with 50 Å and 300 Å are found to give similar results.

3. Results

A schematic for the shear simulations is shown in Fig. 1a and 1b for orientation $\langle 0\bar{1}\bar{1} \rangle$ deformed along the xy angle. The $\langle 01\bar{1} \rangle$ orientation is directed along the z axis. Since NM has an orthorhombic unit cell, each cell angle is initially 90°. As the crystal is sheared, the xy angle decreases while the atoms move simultaneously according to Newton's laws to minimize the energy and forces.

Approved for public release; distribution is unlimited.

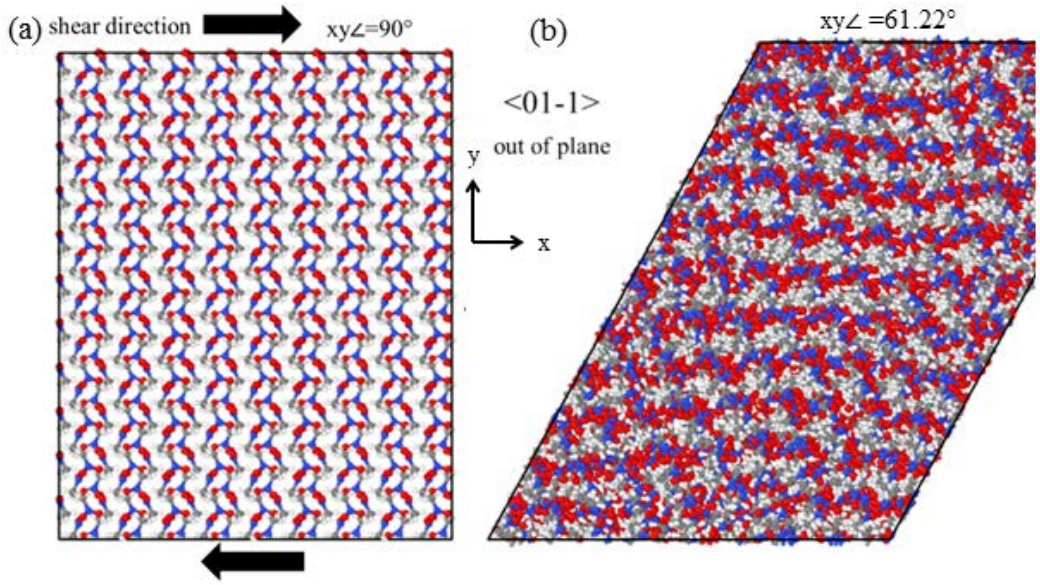

Fig. 1 Schematic of the shear simulations on NM using the single crystal $\langle 01\bar{1} \rangle$ orientation sheared along the xy angle as an example. Initially a) each angle of the simulation box is 90° and then b) the xy angle is reduced to simulate shearing the material. In b) NM has transformed into a disordered state.

The response of NM under shear is highly dependent on the crystallographic orientation. In Fig. 2a the shear stress is given as a function of shear angle for the $\langle 01\bar{1} \rangle$ orientation for the 3 shear directions. This orientation is representative of the results found for many other orientations that are simulated. The shear stress profile is different for all 3 shear directions, but in all cases the shear stress builds up until a maximum shear stress is reached. After the maximum shear stress is reached, the material suddenly transforms into a disordered state as shown in Fig. 1b and the shear stress suddenly drops (see Fig. 2a for shear along the xy angle). In addition to the drop in the shear stress, the transformation to the disordered state is accompanied with a drop in potential energy as shown in Fig. 2b, which is most easily seen for the shear of the xy angle at about 65°. The drop in potential energy corresponds to a sudden increase in kinetic energy. Nevertheless, the rapid increase in kinetic energy does not cause reactions to occur. The magnitude of the maximum shear stress, the shear angle, and the magnitude of the potential energy drop are all highly dependent on the crystallographic orientation and shear direction.

Approved for public release; distribution is unlimited.

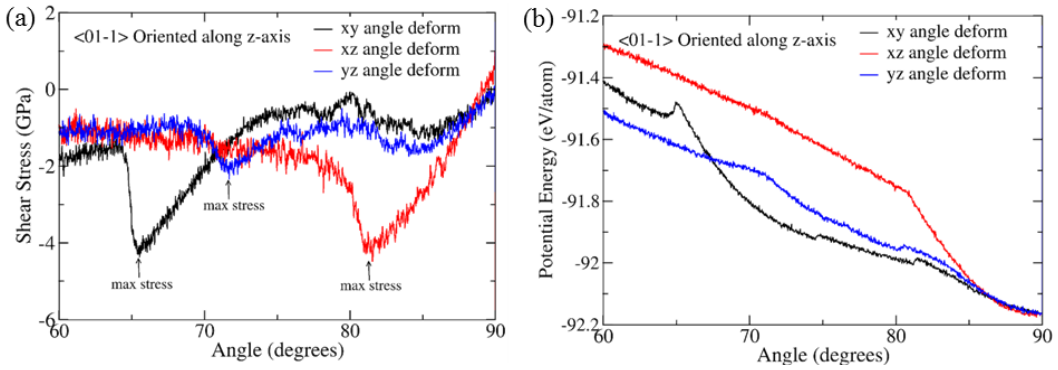

Fig. 2 The a) shear stress Si (xy, xz, or yz) and b) potential energy as a function of shear angle (xy, xz, or yz) during the shear simulation for the $\langle 01\bar{1} \rangle$ orientation of NM. This orientation is chosen to be displayed as a representative example of a large shear stress and large shear angle as well as a low shear stress and low shear angle that occurs in NM during shear.

The orientation dependence can be attributed to the atomistic dynamics that occur in the crystal during shear. For shear along the xy angle, the NM molecules are initially oriented so that they are staggered with respect to one another along the y-axis as shown in Fig. 3a. As the crystal is sheared, the NM molecules rotate so that they are roughly oriented in the same direction, as can be seen in Fig. 3b at 65.77°, which is just before the transformation to the disordered state. The rotation of the molecules is what allows the crystal to be sheared to such a large angle, as shown in Fig. 2a. Once the molecules can no longer rotate, a large shear stress of about 4 GPa builds up, and then the transformation to the disordered state occurs.

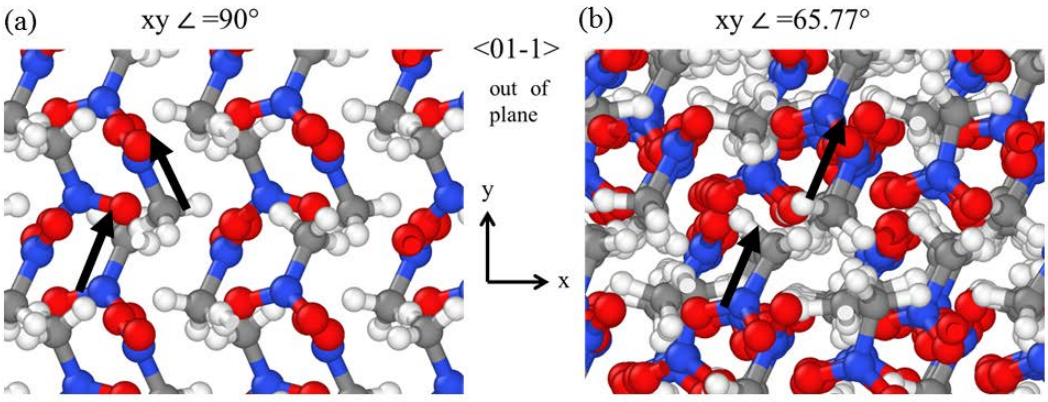

Fig. 3 Zoomed-in snapshots of the NM molecules for the $\langle 01\bar{1} \rangle$ orientation sheared along the xy angle. The NM molecules are a) initially staggered along the y axis, and then after the crystal is sheared b), the NM molecules are rotated to orient themselves in the same direction.

In contrast, when the $\langle 01\bar{1} \rangle$ orientation is sheared along the yz angle, only a small shear stress is built up (about 2 GPa), as shown in Fig. 2a. This is because in addition to the rotation of the NM molecules, the planes of the NM molecules also

shift in the shear direction, reducing the shear stress. The initial configuration of the NM molecules is displayed in Fig. 4a, where the NM molecules are once again staggered along the y axis. Notice that there is some empty space between the "planes" of NM molecules in the xy plane in Fig. 4a. This allows the top plane of NM molecules to shift with respect to the bottom plane during shear. This can be seen by comparing the relative positions of the NM molecules in Fig 4a with those in Fig. 4b, where the y-coordinate of adjacent NM molecules along the z axis are no longer equivalent.

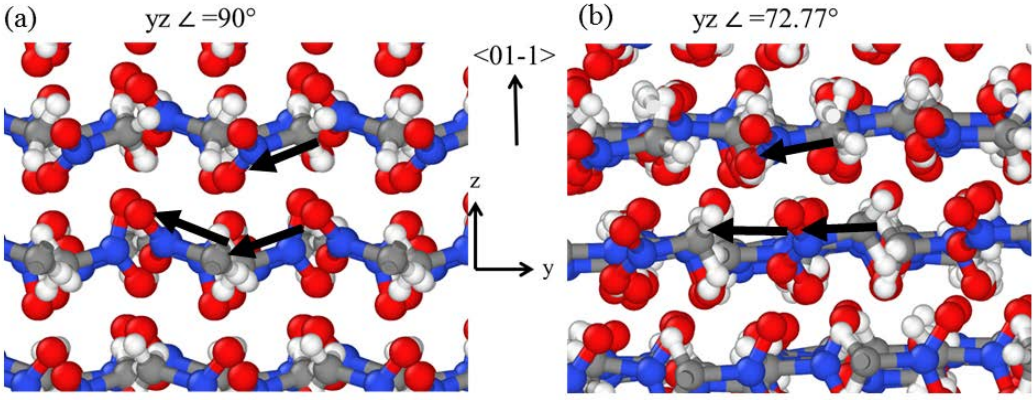

Fig. 4 Zoomed-in snapshots of the NM molecules for the $\langle 01\bar{1} \rangle$ orientation sheared along the yz angle. The NM molecules are initially a) staggered along the y-axis, and the adjacent planes of NM molecules have approximately the same y coordinate. After shear b), the NM molecules are oriented along the same direction, and the adjacent plane of NM has shifted along the y axis.

For all the orientations simulated, the maximum shear stress ranges between 1.68 and 5.24 GPa, and the shear angle ranges from 64.3° to 86.7° as shown in Table 1. The $\langle 01\bar{1} \rangle$ orientation given as an example has a range of 2.35–4.48 GPa and 65.5°–81.5° for the 3 shear directions, so it is a good representative example of the variety of shear dynamics in NM. The orientations that can be sheared to the lowest angles likely have a significant amount of rotation in the NM molecules, such as what is observed in the $\langle 01\bar{1} \rangle$ orientation. In contrast, the orientations that reach the maximum stress near 90° likely do not allow for any rotation of the molecules. At this time it is not clear whether initiation is preferred for orientations with the highest/lowest shear stress or highest shear angle, or if another parameter such as maximum temperature controls the sensitivity in each orientation.

Approved for public release; distribution is unlimited.

Table 1 Summary of the maximum shear stress and the shear angle at maximum shear stress for each single crystal orientation of NM simulated

Orientation $\langle hkl \rangle$	Max $\lvert S_{xy} \rvert$ (GPa)	Shear angle (°)	Max $\lvert S_{xz} \rvert$ (GPa)	Shear angle (°)	Max $\lvert S_{yz} \rvert$ (GPa)	Shear angle (°)
$\langle 0\bar{1}\bar{1} \rangle$	4.21	83.1	5.24	80.8	4.03	81.5
$\langle 10\bar{1} \rangle$	2.15	69.1	2.70	85.2	4.67	82.1
$\langle 11\bar{1} \rangle$	3.73	83.3	3.34	82.9	4.54	82.1
$\langle 110 \rangle$	3.03	66.9	4.53	80.8	2.98	85.2
$\langle 010 \rangle$	3.92	64.7	3.46	85.1	1.95	72.9
$\langle 1\bar{1}1 \rangle$	4.06	82.6	3.03	86.7	2.96	77.1
$\langle 111 \rangle$	4.08	82.7	3.27	76.1	3.01	86.7
$\langle 1\bar{1}0 \rangle$	3.43	68.4	3.46	86.1	2.85	85.1
$\langle 01\bar{1} \rangle$	4.38	65.5	4.48	81.5	2.35	71.6
$\langle 101 \rangle$	2.19	64.3	2.79	84.9	3.51	78.3
$\langle 011 \rangle$	3.07	67.4	2.94	86.6	1.68	72.9
$\langle 001 \rangle$	2.60	67.5	2.77	72.7	4.27	64.9
$\langle 100 \rangle$	4.26	64.6	3.59	66.2	2.54	64.2

In order to include GBs into the simulations, the structure at the GB interface should be similar to what is present in experiment; however the experimental GB structure of NM is currently unknown. To generate realistic GB structures, the following method is used. Several hundred GB structures are generated by creating 3 GBs with different misorientation angles (along z axis) for grains with orientations $\langle h_1 k_1 l_1 \rangle / \langle h_2 k_2 l_2 \rangle$ (along the y axis) where *h*, *k* and *l* range from –1 to 1. A total of 273 GBs are created; however, some of them have the same $\langle hkl \rangle$ orientation and therefore represent a bulk structure with a defect at the interface rather than a real GB. Nevertheless, all the structures are relaxed at 20 GPa and 300 K and ranked according to the GB energy. The following formula is used for the GB energy: $(U_{GB} - U_{perfect})/2A$, where U_{GB} is the GB energy and $U_{perfect}$ is the energy of a perfect, single crystal, and A is the area of the GB. The shear simulations are performed on the 15 best structures with the lowest GB energy.

When a bicrystalline GB is included in the shear simulations, the shear dynamics are more complex; however, the overall process is still similar to the single crystal. The shear stress still builds up followed by a transformation to a disordered state. In Fig. 5a and 5b, the shear stress and potential energy profile during shear are given as a function of shear angle for the $\langle 011 \rangle / \langle 011 \rangle$ orientation along the z axis and $\langle 0\ 27\ \overline{14} \rangle / \langle 0\ \overline{27}\ 14 \rangle$ orientation along the y axis. This corresponds to a misorientation angle of 90° about the z axis. This orientation is chosen as an example because it has similar properties as many of the GBs that are simulated. As shown in Table 2, the maximum shear stresses and the GB energy for this

orientation are similar to many of the orientations simulated, aside from a few outliers.

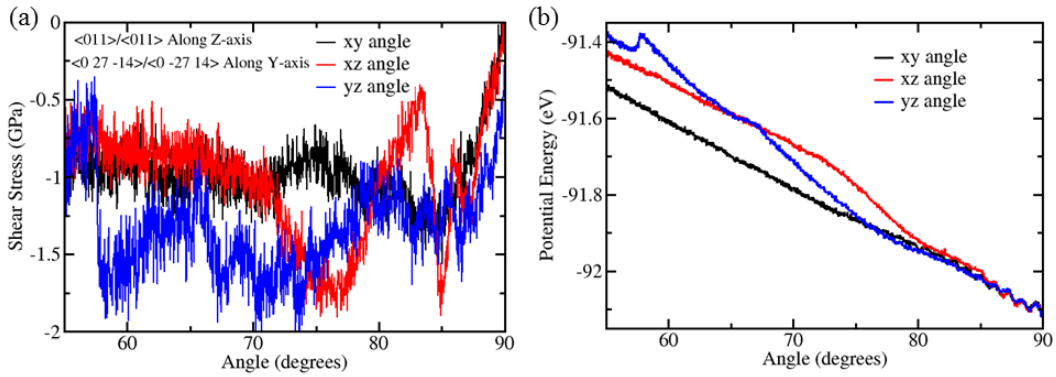

Fig. 5 The (a) shear stress and (b) potential energy given as a function of shear angle for a bicrystalline simulation of NM

Table 2 Summary of the calculated grain boundary (GB) orientations, maximum shear stress, shear angle where the shear stress occurs, and GB energy

Z-axis orientation: $\langle hkl\rangle/\langle hkl\rangle$	Y-axis orientation: $\langle hkl\rangle/\langle hkl\rangle$	GB energy (eV/Å^2)	Max. $\lvert S_{xy}\rvert$ (GPa)	Angle (°)	Max. $\lvert S_{xz}\rvert$ (GPa)	Angle (°)	Max. $\lvert S_{xz}\rvert$ (GPa)	Angle (°)
$\langle 011\rangle/\langle 011\rangle$	$\langle 0\ 27\ \bar{1}4\rangle/\langle 0\ 27\ 14\rangle$	0.903	1.56	85.0	1.91	76.6	2.10	70.6
$\langle 011\rangle/\langle 01\bar{1}\rangle$	$\langle 0\ 27\ \bar{1}4\rangle/\langle 0\ 27\ 14\rangle$	1.025	1.46	70.6	1.76	85.7	2.11	71.6
$\langle 011\rangle/\langle 01\bar{1}\rangle$	$\langle 0\ 27\ 14\rangle/\langle 0\ \bar{2}7\ \bar{1}4\rangle$	0.932	1.33	79.5	1.70	82.5	2.87	60.9
$\langle 1\bar{1}0\rangle/\langle 1\bar{1}0\rangle$	$\langle 3\ 2\ 0\rangle/\langle \bar{4}9\ \bar{3}3\ 0\rangle$	0.867	1.80	85.3	3.64	73.8	1.64	59.7
$\langle 1\bar{1}1\rangle/\langle 1\bar{1}1\rangle$	$\langle 8\ 15\ 5\rangle/\langle \bar{8}\ \bar{1}5\ \bar{5}\rangle$	0.819	2.55	77.2	2.48	82.2	2.06	68.7
$\langle 1\bar{1}1\rangle/\langle 111\rangle$	$\langle \bar{8}\ \bar{1}5\ \bar{5}\rangle/\langle \bar{8}\ 15\ \bar{5}\rangle$	1.246	2.09	78.1	4.15	83.1	1.92	69.7
$\langle 1\bar{1}1\rangle/\langle 11\bar{1}\rangle$	$\langle 8\ 15\ 5\rangle/\langle \bar{8}\ 15\ 5\rangle$	3.111	2.09	80.9	2.55	64.2	1.84	82.9
$\langle 1\bar{1}1\rangle/\langle 11\bar{1}\rangle$	$\langle 8\ 15\ 5\rangle/\langle 8\ \bar{1}5\ \bar{5}\rangle$	0.921	2.14	77.5	2.21	76.6	2.21	65.0
$\langle 1\bar{1}\bar{1}\rangle/\langle 1\bar{1}\bar{1}\rangle$	$\langle \bar{8}\ \bar{1}5\ \ 5\rangle/\langle 8\ 15\ \bar{5}\rangle$	0.698	1.98	82.6	2.60	82.0	1.98	69.3
$\langle 1\bar{1}\bar{1}\rangle/\langle 11\bar{1}\rangle$	$\langle 8\ 15\ \bar{5}\rangle/\langle 8\ \bar{1}5\ \bar{5}\rangle$	0.987	1.71	85.7	3.76	83.4	2.17	67.5
$\langle 1\bar{1}\bar{1}\rangle/\langle 11\bar{1}\rangle$	$\langle 8\ 15\ \bar{5}\rangle/\langle \bar{8}\ 15\ 5\rangle$	0.773	2.00	81.6	2.34	74.9	1.92	69.5
$\langle 111\rangle/\langle 111\rangle$	$\langle 8\ \bar{1}5\ 5\rangle/\langle \bar{8}\ 15\ \bar{5}\rangle$	0.770	1.99	81.8	2.62	81.8	1.90	67.5
$\langle 111\rangle/\langle 11\bar{1}\rangle$	$\langle \bar{8}\ 15\ \bar{5}\rangle/\langle \bar{8}\ 15\ 5\rangle$	0.928	1.85	83.9	2.29	73.5	1.90	71.0
$\langle 11\bar{1}\rangle/\langle 11\bar{1}\rangle$	$\langle \bar{8}\ 15\ 5\rangle/\langle 8\ \bar{1}5\ \bar{5}\rangle$	0.809	2.39	77.9	2.42	70.8	1.91	68.1
$\langle 011\rangle/\langle 011\rangle$	$\langle 0\ \bar{2}7\ 14\rangle/\langle 0\ \bar{2}7\ 14\rangle$	0.449	1.49	85.0	1.73	72.6	2.5	58.4

As shown in Fig. 5a, as this orientation is sheared along the yz angle, the shear stress builds up slowly and even drops slightly around 85°, then builds up again. In this simulation, the grain is slowly rotating with the shear, as displayed in Fig. 6a and 6b. The molecules do not rotate much in the beginning of the simulation, but the grain rotates considerably. This can be seen more clearly by examining the C-N bonds in NM along the arrow shown in Fig. 6a and 6b.

Approved for public release; distribution is unlimited.

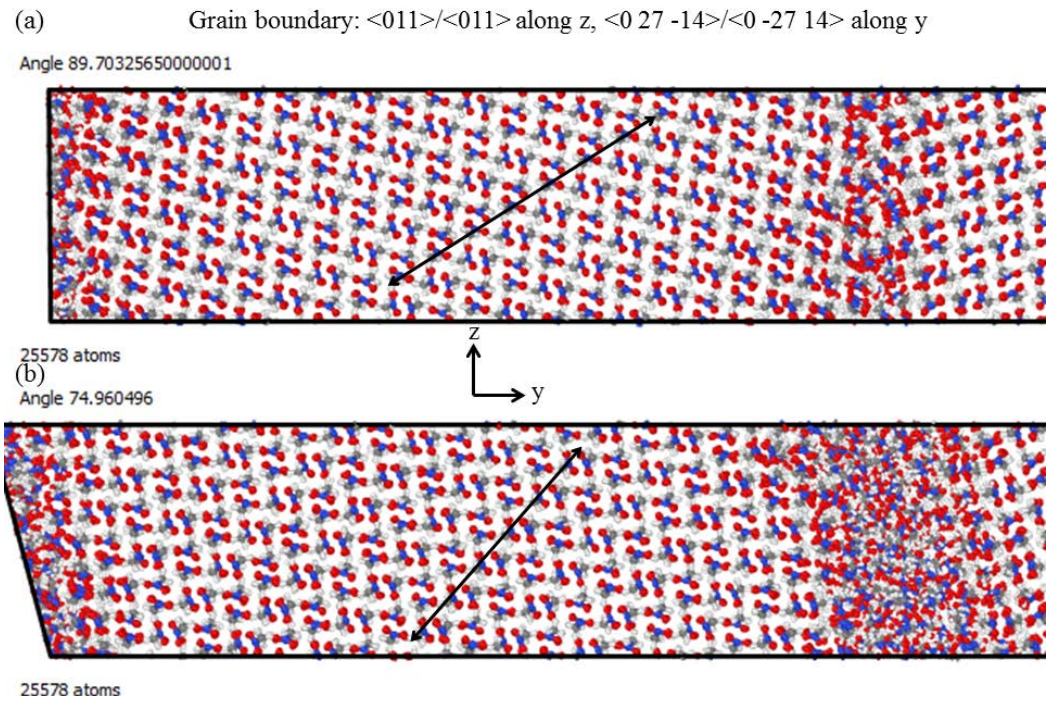

Fig. 6 Snapshots during the shear stress along the yz angle with a bicrystal GB. A line is shown in a) and b) as a guide to the eye to shown the rotation of the grain.

Also shown in Fig. 6a is that the disordered material originates at the GB interface and expands from there as shown in Fig. 6b. However, in stark contrast, when sheared along the xz angle, the entire crystal suddenly transforms into the disordered state, which causes the shear stress to drop rapidly, as shown in Fig. 5a at 85°. Interestingly, the shear stress then rises again. This is because the transformation to the disordered state is incomplete, and the material still maintains a small amount of order. The transformation to the disordered state is not complete until about 75°.

As shown in Table 1, the largest absolute shear stress is found to occur in the $\langle 0\bar{1}1\rangle/\langle 111\rangle$ orientation along z and $\langle \bar{8}\ \bar{15}\ \bar{5}\rangle/\langle \bar{8}\ 15\ \bar{5}\rangle$ along y sheared along the xz axis of 4.15 GPa at an angle of 83.1°. However, in spite of the large build-up of shear stress, no reactions are observed in this bicrystalline simulation, which is similar to what is found for the single crystal simulations.

4. Conclusions

The short time-scale dynamics during shear of NM have been revealed using molecular dynamics simulations. Shear simulations have been performed using single crystals with a range of orientations and shear directions as well as bicrystals,

also with a range of orientations and misorientation angles. Although no chemical reactions are observed during the simulations, the dynamics presented are possibly associated with the short time-scale reaction pathway that leads to initiation. In this sense, these results are critical for understanding the complete mechanism for initiation of NM under shear stress.

Since no reactions are observed in the simulations but are observed in experiment, the future work is mostly geared toward resolving this intriguing discrepancy as well as generally increasing the length and time scales, and the range of orientations studied. The initiation may be related to the presence of multiple GBs, so simulations with polycrystalline NM may be important. Investigating the size-dependence of the results more thoroughly with GBs may also be needed because the GB simulations require that the size of the grain be much larger than the size of the GB. In addition, initiation may be related to the slip and subsequent momentum transfer of grains much larger than what is simulated, so the size-dependence needs to be investigated thoroughly. The time scale of the simulations may also be an issue because it may be that the time scale for reactions to occur is simply larger than the time scales simulated. An analysis of activation energies and Arrhenius reaction rates for proposed reactions may yield an estimate of the time scale needed. A greater variety of GB orientations can also be simulated, which may yield interesting results. All the results presented are at 20 GPa; it would be interesting to examine the pressure dependence of the results, since there is a clear pressure dependence in the experiment related to the reaction threshold pressure.

This work was conducted as part of the DOD High Performance Computing Modernization Program's (HPCMP's) Workforce Development initiative and is aimed at providing the future science and engineering workforce the computational skills and experience necessary to close the gap between the technological capability and computational skills necessary to support the DOD's future Warfighter needs. The HPCMP's 2016 Internship Program was a valuable experience for Brad Steele, and the impact of the summer research experience on his professional career is discussed in the Appendix.

Approved for public release; distribution is unlimited.

5. References

1. Citroni M, Datchi F, Bini R, Di Vaira M, Pruzan P, Canny B, Schettino V. Crystal structure of nitromethane up to the reaction threshold pressure. J Phys Chem B. 2008;112(4):1095–1103.

2. Citroni M, Bini R, Pagliai M, Cardini G, Schettino V. Nitromethane decomposition under high static pressure. J Phys Chem B. 2010;114(29): 9420–9428.

3. Guo F, Cheng X-l, Zhang H. Reactive molecular dynamics simulation of solid nitromethane impact on (010) surfaces induced and nonimpact thermal decomposition. J Phys Chem A. 2012;116(14):3514–3520.

4. Dick JJ. Orientation-dependent explosion sensitivity of solid nitromethane. J Phys Chem. 1993;97(23):6193–6196.

5. Hébert PA, Isambert A, Petitet J-P, Zerr A. Raman spectroscopy study of nitromethane in a shear diamond anvil cell. High Pressure Research. 2010;30(1):24–27.

6. Manaa RM, Reed EJ, Fried LE, Galli G, Gygi F. Early chemistry in hot and dense nitromethane: molecular dynamics simulations. J Chem Phys. 2004;120(21):10146–10153.

7. Nelson T, Bjorgaard J, Greenfield M, Bolme C, Brown K, McGrane S, Scharff RJ, Tretiak S. Ultrafast photodissociation dynamics of nitromethane. J Phys Chem A. 2016;120(4):519–526.

8. Courtecuisse S, Cansell F, Fabre D, Petitet JP. Phase transitions and chemical transformations of nitromethane up to 350 °C and 35 GPa. J Chem Phys. 1995;102(2):968–974.

9. Plimpton S. Fast parallel algorithms for short-range molecular dynamics. J Comp Phys. 1995;117(1):1–19.

10. Larentzos JP, Rice BM, Byrd EFC, Weingarten NS, Lill JV. Parameterizing complex reactive force fields using multiple objective evolutionary strategies (MOES). Part 1: ReaxFF models for cyclotrimethylene trinitramine (RDX) and 1,1-diamino-2,2-dinitroethene (FOX-7). J ChemTheory and Computation. 2015;11(2):381–391.

11. Rice BM, Larentzos JP, Byrd EFC, Weingarten NS. Parameterizing complex reactive force fields using multiple objective evolutionary strategies (MOES): Part 2: transferability of ReaxFF models to C–H–N–O energetic materials. J Chemical Theory and Computation. 2015;11(2):392–405.

12. Strachan A, van Duin ACT, Chakraborty D, Dasgupta S, Goddard WA. Shock waves in high-energy materials: the initial chemical events in nitramine RDX. Physical Review Letters. 2003;91(9):098301.

13. Zhang L, Zybin SV, van Duin ACT, Dasgupta S, Goddard WA, Kober EM. Carbon cluster formation during thermal decomposition of octahydro-1,3,5,7-tetranitro-1,3,5,7-tetrazocine and 1,3,5-triamino-2,4,6-trinitrobenzene high explosives from ReaxFF reactive molecular dynamics simulations. J Phys Chem A. 2009;113(40):10619–10640.

Approved for public release; distribution is unlimited.

INTENTIONALLY LEFT BLANK.

Appendix. Impact of Summer Research Experience

Approved for public release; distribution is unlimited.

The following remarks were made by Brad Steele in reference to his experience as a student intern at ARL under the 2016 HPCMP Internship Program.

Background

I am a PhD candidate at the University of South Florida, Physics Department, where I earned my MS in Applied Physics. I have a significant amount of experience performing density functional theory calculations and bash scripting and programming for running large amounts of simulations and data analysis. My past research experience dealt with predicting and characterizing new kinds of materials at high pressures. This involves zero-temperature energy-minimization calculations to determine thermodynamic and dynamical stability. I have much less experience performing simulations using LAMMPS and analyzing time-dependent dynamical results. My goals for participating in the internship were to gain more experience using LAMMPS and analyzing dynamical results. Furthermore, I wanted to gain experience conducting research at a government research lab to understand the techniques and how research challenges are tackled on a government level.

Impact

The HPCMP Internship Program has been incredibly useful for me. I have gained a tremendous amount of experience running molecular dynamics simulations and analyzing the results. I have also been able to further develop my programming and bash scripting skills. More significantly, I have a much better appreciation for what molecular dynamics is capable of and what its limitations are. Before this internship, I had never used ReaxFF; I now recognize its potential. Furthermore, I have a much better understanding of the technical terms used by the energetic materials community and what types of properties they are interested in. One thing that surprised me about my project was how difficult it is to get the metastable molecules to react. I had generally assumed that chemical reactions can be observed easily using molecular dynamics, but that is not the case. I have also gained an appreciation of what researchers mean when they say a material reacts or decomposes under some sort of stress, why the response of the material depends on the type of stress applied, and why the rate of the reaction is very important factor for energetic materials. On a personal level, this experience is of tremendous value to me because I want to work at a government lab when I graduate. It has been very good to meet the other researchers and learn about what they are working on and how they are trying to solve their research problems. This program also fulfills a necessary requirement for my PhD.

Approved for public release; distribution is unlimited.

List of Symbols, Abbreviations, and Acronyms

GB	grain boundary
HPCMP	High Performance Computing Modernization Program
LAMMPS	Large-scale Atomic/Molecular Massively Parallel Simulator
MOES	Multiple Objective Evolutionary Strategies
NM	nitromethane (CH_2NO_3)

1 (PDF) DEFENSE TECHNICAL INFORMATION CTR DTIC OCA

2 (PDF) DIRECTOR US ARMY RESEARCH LAB RDRL CIO L IMAL HRA MAIL & RECORDS MGMT

1 (PDF) GOVT PRINTG OFC A MALHOTRA

2 (PDF) UNIV OF SOUTH FLA DEPT OF PHYSICS B STEELE I OLEYNIK

4 (PDF) HIGH PERFORM CMPTG MODERNIZATION PROG OFC S BELL C DAHL L DAVIS D SCHWARTZ

7 (PDF) DIR USARL RDRL WML B T JENKINS J P LARENTZOS W MATTSON B RICE N S WEINGARTEN N TRIVEDI RDRL WMM F S COLEMAN